Cryo-Atomic Force Microscopy of Smooth Muscle Myosin

Yiyi Zhang,* Zhifeng Shao,* Andrew P. Somlyo,*§ and Avril V. Somlyo*#
Departments of *Molecular Physiology and Biological Physics, #Pathology and §Medicine, University of Virginia Health Sciences Center, Charlottesville, Virginia 22906-0011 USA

ABSTRACT The motor and regulatory domains of the head and the 14-nm pitch of the α-helical coiled-coil of the tail of extended (6S) smooth-muscle myosin molecules were imaged with cryo atomic force microscopy at 80–85 K, and the effects of thiophosphorylation of the regulatory light chain were examined. The tail was 4 nm shorter in thiophosphorylated than in nonphosphorylated myosin. The first major bend was invariant, at ~51 nm from the head-tail junction (H-T), coincident with low probability in the paircoil score. The second major bend was 100 nm from the H-T junction in nonphosphorylated and closer to a skip residue than the bend (at 95 nm) in thiophosphorylated molecules. The shorter tail and distance between the two major bends induced by thiophosphorylation are interpreted to result from melting of the coiled-coil. An additional bend not previously reported occurred, with a lower frequency, approximately 24 nm from the H-T. The range of separation between the two heads was greater in thiophosphorylated molecules. Occasional high-resolution images showed slight unwinding of the coiled-coil of the base of the heads. We suggest that phosphorylation of MLC_{20} can affect the structure of extended, 6S myosin.

INTRODUCTION

The crystal structures of subfragment-1 (S1) of skeletal-muscle myosin (Rayment et al., 1993b) and of the regulatory domain of Ca-regulated scallop myosin (Xie and Cohen, 1994) have provided major new insights into the workings of the myosin motor. Rayment and colleagues (1993b) suggested that the C-terminus of the long α-helix stabilized by the essential (ELC) and regulatory (RLC) light chains serves as a lever arm that translates small-scale conformational movements in the catalytic and actin-binding motor domain into the nanometer movement expected of the swinging cross-bridge (Rayment et al., 1995; Houdusse and Cohen, 1995). Indeed, tilting of the light-chain region of smooth-muscle S1-decorated actin has been detected in the presence of MgADP by cryo-electron microscopy (Whittaker et al., 1995). However, studies of S1 cannot reveal the structure or possible movement at the head-rod junction or the relationship and possible interactions between the regulatory domains of the two-headed myosin molecule. Both heads and a segment of tail are required for regulation of smooth-muscle and scallop-muscle myosins in which phosphorylation or Ca binding to the RLCs, respectively, serves as the "on" switch: S1 or myosin lacking a RLC on one head is in the "on state," and interaction of both heads (Stafford et al, 1979; Ikebe and Hartshorne, 1985; for a review, see Vibert and Cohen, 1988), together with a portion of the coiled-coil region, is required for the "off state" (Trybus, 1994; Matsu-ura and Ikebe, 1995).

Electron microscopy of metal-shadowed (Elliott and Offer, 1978; Winkelmann and Lowey, 1986; Suzuki et al., 1985; Flicker et al., 1983) or negatively stained myosin molecules (Walker et al., 1985, 1991) has been widely and successfully used to demonstrate the flexibility of the myosin heads, the location of the light chains, and both 10S (looped) and 6S (extended) conformations of smooth-muscle myosin. However, metal shadowing of molecules degrades the resolution; negative staining of myosin is difficult and imposes the effect of the stain on protein conformation (Walker et al., 1991). The use of an alternative approach, atomic force microscopy (AFM), that is subject to different limitations, now provides the means to confirm or negate and, it is hoped, extend the results obtained with electron microscopic techniques.

The recently developed cryo-atomic force microscope (cryo-AFM) (Mou et al., 1993; Han et al., 1995; Shao et al., 1995; Zhang et al., 1996) combines high resolution with the high contrast that obviates the need for, but does not preclude the use of, image processing for resolving the structure of single, isolated molecules at nanometer resolution. Surface contamination (Prater et al., 1991) is virtually eliminated by operating the AFM in liquid nitrogen vapor, and the rigidity of most biological macromolecules is significantly greater at about 80 K than at room temperature (Han et al., 1995). Because of this improved rigidity, tip-induced deformation of the molecules is also much reduced when compared with AFM imaging at room temperature, enabling the use of the very sharp tips required for high resolution. At cryogenic temperatures, the thermal motion of flexible or mobile macromolecules (Thomson et al., 1996) is also minimized, their adhesion to the substrate increased, and bare (unstained and unshadowed) molecules can be conveniently imaged without tip-induced movement (Zhang et al., 1996).

Received for publication 7 October 1996 and in final form 11 December 1996.

Address reprint requests to Dr. Z. Shao or Dr. A. V. Somlyo, Department of Molecular Physiology and Biological Physics, University of Virginia Health Sciences Center, P. O. Box 10011, Charlottesville, VA 22906-0011. Tel.: 804-982-0825; Fax: 804-982-1616; E-mail: avs5u@elvis.med.virginia.edu.

0006-3495/97/03/1308/11 $2.00

We used cryo-AFM at temperatures between 80 and 85 K to image thiophosphorylated and nonphosphorylated smooth-muscle myosin maintained in the physiologically relevant, 6S conformation by high concentration of ammonium acetate (Onishi and Wakabayashi, 1982), and resolved the two-headed structure and its helical tail with excellent stability. In some views, where the two heads were well separated, the regulatory domain of the myosin head associated with the light chains could be directly imaged, indicating that a spatial resolution of 3–5 nm was attained without image processing. The head-neck junction appeared somewhat more flexible, and the total length of the myosin tail was 4 nm shorter in the thiophosphorylated molecules; this difference could be accounted for by the 5-nm difference in the distance between the two major bends occurring approximately one-third and two-thirds along the length of the tail. In nonthiophosphorylated molecules the position of the third bend shifted to a position closer to the skip residue that favors the 10S conformation. The helical modulation of the coiled-coil tail was also discernible in images obtained with high-resolution tips.

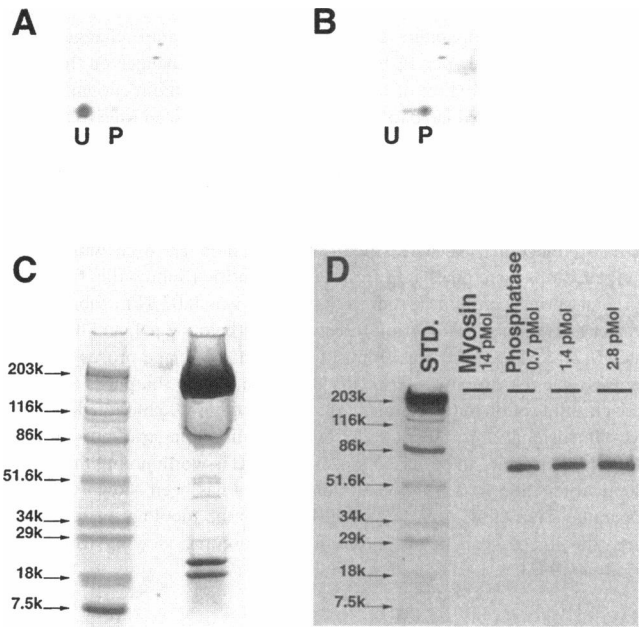

FIGURE 1 Characterization of the nonphosphorylated and thiophosphorylated myosin used for AFM imaging. *A* and *B* show two-dimensional gel electrophoresis of nonphosphorylated (*A*) and thiophosphorylated (*B*) turkey gizzard myosin stained with colloidal gold (Kitazawa et al., 1991). Densitometry of the gels indicated that the level of phosphorylation was less than 5% in the nonphosphorylated and greater than 95% in the thiophosphorylated myosins. (*C*) One-dimensional SDS gel intentionally heavily loaded with myosin and stained with Coomassie colloidal burst, showing the absence of significant amounts of contaminant proteins. The overloaded myosin heavy chain seen at about 203 kDa, and the regulatory and essential light chain at 20 and 17 kDa, respectively, are the major proteins. (*D*) Western blot of the same sample of myosin as used for AFM studies, heavily loaded as in *C* and reacted with a monoclonal antibody (kindly provided by Dr. David Hartshorne, University of Arizona) to the smooth muscle-specific phosphatase (SMPP-1 M) regulatory subunit (110 kDa) to test for contamination of the myosin with SMPP-1 M, which would complicate the interpretation of the AFM images. Recombinant phosphatase purified from a partial length clone of 72 kDa SMPP-1 M (Haystead et al., 1995) was loaded at three different concentrations as a control. SMPP-1 M (7 pmol) was detected, and therefore we conclude that any phosphatase contamination of the myosin is significantly less than 20-fold.

MATERIALS AND METHODS

Protein preparation

Turkey gizzard myosin, 70% SM2 and 30% SM1 heavy chain isoforms, was a gift from Dr. Kathy Trybus (Brandeis University). This was prepared as previously described (Trybus, 1994) and stored at −20°C in buffer A containing 0.3 M KCl, 10 mM KH_2PO_4, 1 mM EGTA, 1 mM EDTA (pH 6.8), 1.0 mM dithiothreitol, and 50% glycerol. Myosin was thiophosphorylated with ATPγS by standard procedures (Ikebe and Hartshorne, 1986), resulting in thiophosphorylation of light chains of approximately 1 mol of phosphorus/mol of light chain (Fig. 1, *A* and *B*) measured by 2-D electrophoresis (Kitazawa et al., 1991). Difficulty in interpretation of the AFM images could arise from the presence of myosin-associated proteins such as the myosin phosphatase, SMPP-1 M. Therefore, contamination of the myosin by SMPP-1 M was analyzed by Western blot using a monoclonal antibody (kindly provided by Dr. David Hartshorne, University of Arizona) to the SMPP-1 M 110-kDa regulatory subunit. No phosphatase was detected on the lanes heavily loaded with myosin (14 pmol) and stained with Coomassie blue (Fig. 1 *C*) or blotted with the SMPP-1 M antibody (Fig. 1 *D*), whereas phosphatase prepared from a partial clone (72 kDa) of the regulatory subunit (Haystead et al., 1995) showed a dense band, even at the lowest concentration loaded onto the gel (0.7 pmol).

Myosin preparations were extensively dialyzed for 4 to 5 h at 4°C against buffer A without glycerol, because even traces of glycerol resulted in surface contamination and an increase in adhesion force during AFM imaging (Yang and Shao, 1993). In some preparations, myosin aggregates were removed by centrifugation at 130,000 × *g* for 15 min at 4°C. Specimen contamination was reduced by filtering all buffers with 0.22-μm filters.

Specimen preparation

Dialyzed myosin was diluted in 250 mM ammonium acetate at pH 7.2 to a final concentration of ~2 μg/ml immediately before placing 2 μl of the solution on mica freshly cleaved under clean dry nitrogen and incubated on the mica surface for 15 min at room temperature, followed by flushing with 1 ml of 250 mM ammonium acetate at pH 7.2. The effect of H_2O rinse was also examined. Excess solution on the mica surface was rapidly removed by a stream of clean nitrogen gas, and the specimen was lowered into the liquid nitrogen gas chamber surrounding the cryo-AFM. Care was taken that all samples were treated identically. We note that surface water on mica is not completely removed under these conditions (Elmer, 1980). This basic procedure was very similar to that used for rotary-shadowed molecules for electron microscopic studies (Tyler and Branton, 1980), although no spray, glycerol, or metal shadowing was required, and imaging was performed in an ambient nitrogen environment, rather than a vacuum.

Cryo-AFM imaging

The cryo-AFM used in this study, designed and constructed in this laboratory, is described in detail elsewhere (Mou et al., 1993; Shao et al., 1995); it permits replacement of the specimen and cantilever in situ without changing the temperature. The AFM was operated in liquid nitrogen vapor at a pressure slightly higher than the atmospheric pressure. The imaging temperature can be varied between 77 K and 220 K, but for these studies it was maintained at 80–85 K by placing the AFM about 3–5 inches above the liquid nitrogen surface. The variation introduced by the sensitivity of the piezo scanner to changes in temperature (the temperature sensor is

located on the AFM body rather than on the sample surface) was less than 1.1% for a 1 K temperature change, and the temperature change in the AFM is less than 2 K per 12-h period. Temperature changes on the order of 3 K (equivalent to 18 h of operation, assuming a unidirectional change in temperature) would have to occur over the 30-min scan time to account for the 4-nm changes in tail length reported here. The temperature stability, which is better than 4 mK/min, is routinely monitored and has been reported in detail previously (Mou et al., 1993; Shao et al., 1995). Therefore, sample distortion would be less than 0.001% over the 30-min period of data collection. The bare silicon nitride cantilevers used with oxide-sharpened tips were purchased from Park Scientific (Sunnyville, CA). The nominal spring constant at room temperature was 0.03 N/m (about 15% greater at 100 K). The adhesion force was kept below 2 nN, and the frame rate (512 × 512 pixels) was from 5 to 50 min; no image processing was applied. The resolution was critically dependent on the sharpness of the tip and cleanliness of the specimen. The instrument was calibrated using a two-dimensional 1-μm period dot matrix calibration grid provided by Digital Instruments and tobacco mosaic virus. It is worth noting that under identical conditions, 0.5-nm resolution on mica has been shown with this apparatus (Han et al., 1995). As AFM records the topology of the specimen, the images can be displayed for stereoscopic viewing (Shao and Somlyo, 1995).

Specimen measurements

Images were enlarged on the computer screen so that a myosin molecule was approximately 10 cm long. The length-measuring tool in the software for the Nanoscope (Digital Instruments), which allows one to make end-over-end steps of varying length, was used to measure the myosin tail lengths starting at the head-neck junction. Small steps were taken for curved regions, to maintain the measurement line centered along the tail. The differences in tail lengths and bending positions in the tail were not expected and were initially made for comparison with bending positions of 10S myosin. The differences only became apparent after all of the measurements were made and the data plotted, thus decreasing the likelihood of investigator bias.

To check the precision of the measurements, the tail lengths were remeasured by the same investigator. A similar difference was found in both sets of measurements on the 222 nonphosphorylated and 248 phosphorylated molecules.

The probability of coiled-coil structure in the myosin tail was based on the program of Berger et al. (1995), obtainable through paircoil@theory.lcs.mit.edu.

RESULTS

Dimensions of nonphosphorylated and thiophosphorylated myosin molecules

Typical low-magnification cryo-AFM images of fields of thiophosphorylated and nonphosphorylated myosin molecules are shown in Fig. 2, *A* and *B*, respectively. These full-frame images were collected in 30 min at 84 K. Because of the exceptional thermal stability of the system, no apparent distortion was found. The two heads and the tail of many of the molecules are well resolved and similar in appearance to images of rotary-shadowed or negatively stained molecules (Elliot and Offer, 1978; Flicker et al., 1983; Suzuki et al., 1985; Winkelmann and Lowey, 1986; Walker et al., 1991).

Occasionally, aggregates of myosin molecules were observed that had a bipolar appearance, with the tails of the molecules oriented in a parallel fashion (Fig. 3).

The length of the myosin tail was measured starting at the head-neck junction in 222 nonphosphorylated and 248 thiophosphorylated myosin molecules, from five samples, after calibration with both tobacco mosaic virus and a grid of known dimensions. The length distribution was fit to Gaussians (Fig. 4) with a centroid at 154 nm for the nonphosphorylated and 150 nm for the thiophosphorylated myosin. The shortening of the tail upon thiophosphorylation was significantly different ($p < 0.0001$) when both populations were compared using the Mann-Whitney test; the median values were also significantly different ($p < 0.05$, Mann-Whitney test and the Resampling test; $p < 0.03$, Student's

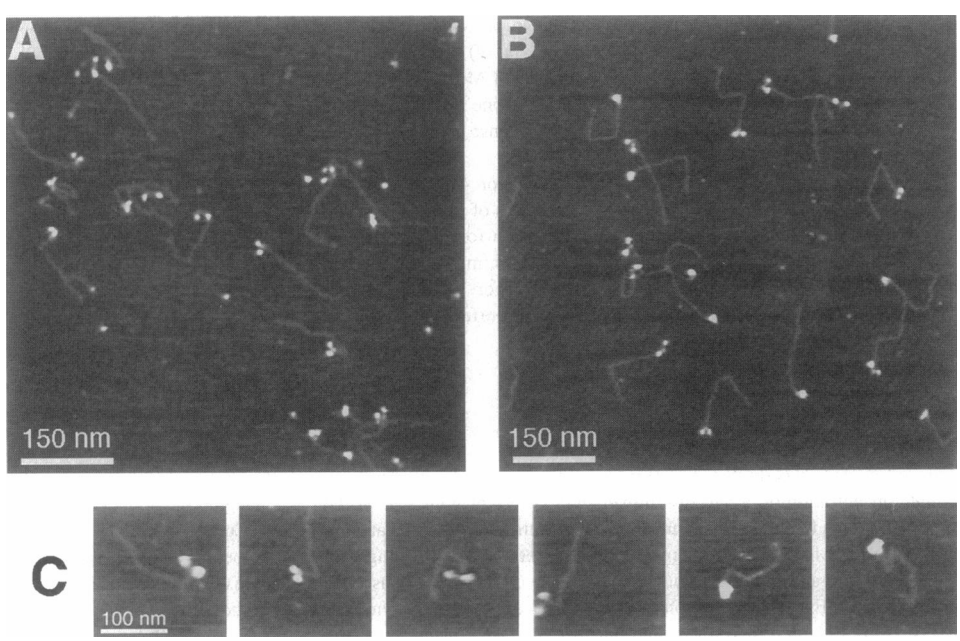

FIGURE 2 Typical fields of thiophosphorylated (*A*) and nonphosphorylated (*B*) smooth muscle myosin molecules imaged with cryo-AFM at 88 K. The adhesion force was kept below 2 nN, and an image (512 × 512 pixels) was completed in 30 min. No image processing was applied. Note the different orientations of the individual heads, reflecting the flexibility of the head-tail junction. The height displacements of the tip resulting in the topological image are displayed on a gray scale, with white being the highest point (10 nm). (*C*) Representative molecules showing the novel bending site 24 nm from the head-neck junction.

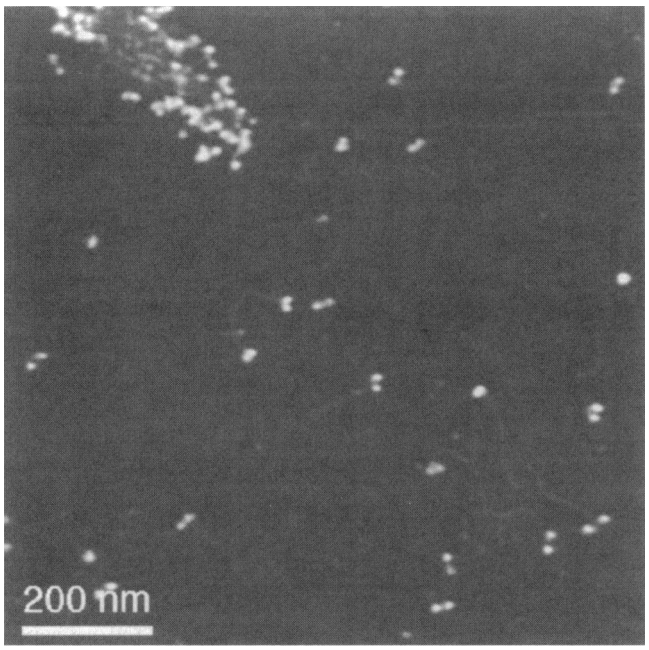

FIGURE 3 A cryo-AFM image (512 × 512 pixels) showing an aggregate of myosin molecules. These occasional aggregates had a bipolar appearance, with the myosin heads on the surface of the aggregate and the tails tending to a parallel arrangement.

t-test). Remeasurement of all the molecules resulted in length distributions with centroids at 155 and 150 nm ($p < 0.03$, Mann-Whitney test) for nonphosphorylated and thiophosphorylated molecules, respectively.

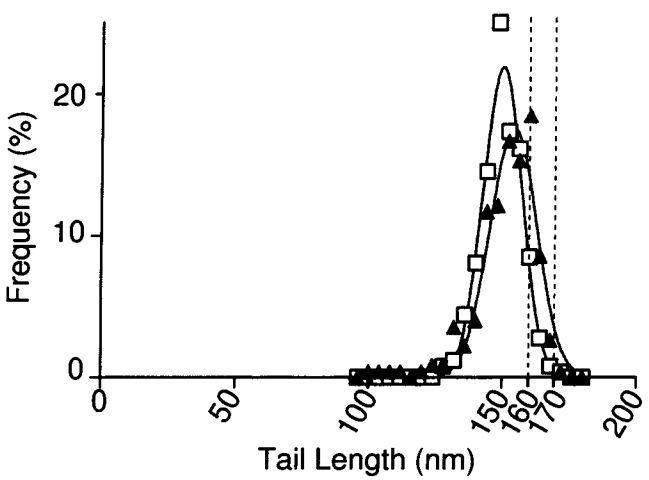

FIGURE 4 Frequency distribution of the myosin tail lengths measured for 223 nonphosphorylated (▲) and 249 thiophosphorylated (□) myosin molecules from five samples. The dotted line at 161 nm indicates the predicted length of the chicken gizzard myosin tail based on the α-helical/coiled-coil onset at Pro 848 and extending to amino acid 1935 for SM-2, assuming a helical rise of 0.148 nm/residue for an α-helical/coiled-coil. The tail lengths between the dashed line at 161 nm and 170 nm would include the 30% of SM-1 molecules that have an additional 40 amino acids at the COOH terminus, giving rise to an additional 6-nm tail length.

Some molecules showed well-defined bends that occurred at three sites along the tail. The frequency of bending and the distribution of the locations of the bends, measured from the bifurcation of the two heads in nonphosphorylated and thiophosphorylated myosin, are shown in Fig. 5. For comparison, the probability of coiled-coil structure (Berger et al., 1995) arising from the well-known heptad repeats in the two α-helices of the myosin tail (McLachlen and Karn, 1983), is plotted as a function of the amino acid sequence starting from the invariant proline (848, region I) to the COOH terminus (Fig. 5 *A*). The skip residues, which are previously suggested (Offer, 1990) points of instability, are also shown. Gaussians were fit to the data to obtain the frequency distributions of the distances from the head-neck

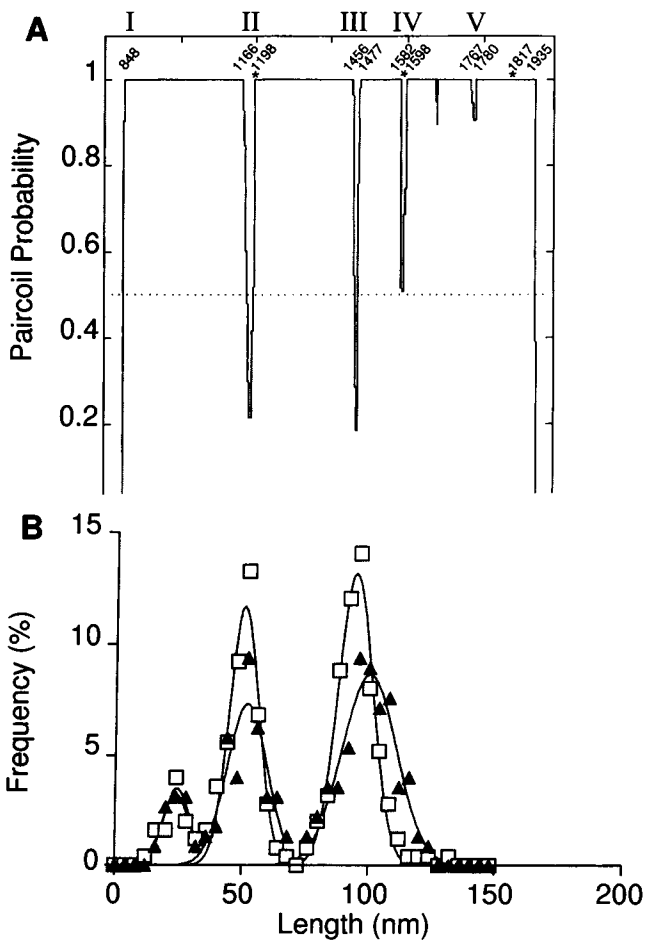

FIGURE 5 Frequency distribution of the position of the bends in the tail (*B*) of nonphosphorylated (▲) and thiophosphorylated (□) myosin. The 0 position on the abscissa represents the head-neck junction (*B*). (*A*) Probability of coiled-coil structure in the tail region using a paircoil probability program (Berger et al., 1995) obtained from paircoil@theory.lcs.mit.edu. The residue numbers are indicated along the top of the graph, as well as the skip residues at 1199, 1592, and 1817 indicated by *. For purposes of discussion in the text, the regions of low probability for coiled-coil structure are indicated by Roman numerals. Based on a helical rise of 0.148 nm/residue for an α-helical coiled-coil, the bend at position 2 would occur at 48–51 nm from proline 848, and this has been aligned with the data in *B*. Myosin sequence from Yanagisawa et al. (1987).

junction to the bending positions. The centroid of the first bend occurred at 24 nm in 10% of both the thiophosphorylated and nonphosphorylated molecules (see Fig. 2 *C*). This bend has not been previously reported. The second bend (first major bend; region II) occurred at 51–52 nm in both thiophosphorylated and nonphosphorylated molecules, at the same distance identified by Onishi and Wakabayashi (1982) as the site of the hairpin bend present in 80% of 10S molecules. The absence of the hairpin in the present study is probably the result of the preparatory procedures: in the presence of high concentrations of ammonium acetate, myosin molecules contain no intramolecular loops (Onishi and Wakabayashi, 1982), and high ionic strength solutions, in general, maintain nonphosphorylated myosin in the extended, 6S conformation (Trybus and Lowey, 1984).

The position of the third bend shifted toward the head-tail junction with thiophosphorylation; its centroid was at 95 nm, compared with the centroid at 100 nm in nonphosphorylated molecules. We interpret this shift, which shortened the distance between the second and third bend, to be consistent with the shorter total length of the tail. When truncated data containing only this part of the measurement were subjected to Student's *t*-test with or without Welch's correction, p was 0.0004, suggesting that the difference in the means is significant, although with the Mann-Whitney test, p was 0.1, perhaps because of the truncation of data where a good Gaussian fit could not be found. Therefore, we made a further comparison of the data truncated at 75 nm using the resampling test, which gave a difference in the means of 4.2 nm with a significant difference of $p < 0.02$. Both major bends occurred with higher frequency in thiophosphorylated molecules (Fig. 5 *B*).

The length and width of the motor domain of individual myosin heads are shown in Table 1. Two populations of 40 molecules each from nonphosphorylated and thiophosphorylated molecules, imaged at higher magnification with the individual heads well resolved in stereo views, were selected for measurements of the height of the motor and regulatory domains of the head. More detailed measurements of 11 heads in seven molecules in which the heads were well resolved in stereo views (Fig. 6, *a1, a2, b1, c2, h1, i1, k1*) indicated that the length of the motor domain represented 54% of the total head length, and the width of the regulatory domain was 56% of the width of the motor domain. The very small, albeit statistically significantly larger, size of the phosphorylated heads in three dimensions is not further considered here, as we believe that the interpretation of these findings will require further exploration with high-resolution measurements.

The width of the tail measured in high-resolution imaging was about 3.6 nm, slightly broader than the known value, 2 nm, of two-stranded α-helical coiled-coils.

Head orientations

To address the question of whether thiophosphorylation of the regulatory light chain changes the head-to-head and head-to-tail relationships, the angle between the two heads measured from the intercept of two lines drawn through the long axis of each head was determined after suitable enlargement of the molecules on the computer screen. The myosin molecules adsorbed to the mica surface showed numerous different orientations. Comparison of nonphosphorylated and thiophosphorylated myosin showed a significant difference in the number of myosin molecules in which the two heads were closely associated (so no separation angle could be measured), as well as in the number of heads separated by 180°, with the thiophosphorylated heads favoring the more separated state. The heads were closely associated in 30% of the 400 nonphosphorylated myosin molecules measured, compared to 21% of 488 thiophosphorylated molecules. Likewise, 20% of the thiophosphorylated myosin heads, compared with 12% of the nonphosphorylated heads, were separated by 180°. Thiophosphorylation, therefore, favored greater separation of the two heads of the molecule, but the change was not dramatic.

Heads bent backward ("flexed") toward the tail were not seen in the present study, probably because this conformation is rarely seen in high-ionic-strength solutions (Suzuki et al., 1985), and because our specimens were prepared by depositing, rather than spraying (Onishi et al., 1983), myosin onto the grids.

Morphology

A gallery of 22 myosin molecules in which the heads are well resolved is shown in stereoscopic views in Fig. 6. In end-on views in which the two heads appear separated by about 180°, such as *a1*, *g1*, *h1*, and *k1*, the regulatory domain of each head is well resolved. The orientation of the heads can be understood more clearly by viewing stereo-

TABLE 1 Head dimensions (nm ± SD)

	Nonphosphorylated		Thiophosphorylated	
	n		*n*	
Length	166	18.0 ± 2.5	182	18.7 ± 2.3
Motor domain width	140	9.0 ± 1.6	160	9.5 ± 1.6
Motor domain height*	40	2.5 ± 0.37	40	3.0 ± 0.41
Regulatory domain height*	40	1.3 ± 0.19	40	1.4 ± 0.35

n, Number of molecules measured. *The height measurement does not include the portion of the structure embedded in surface adsorbent.

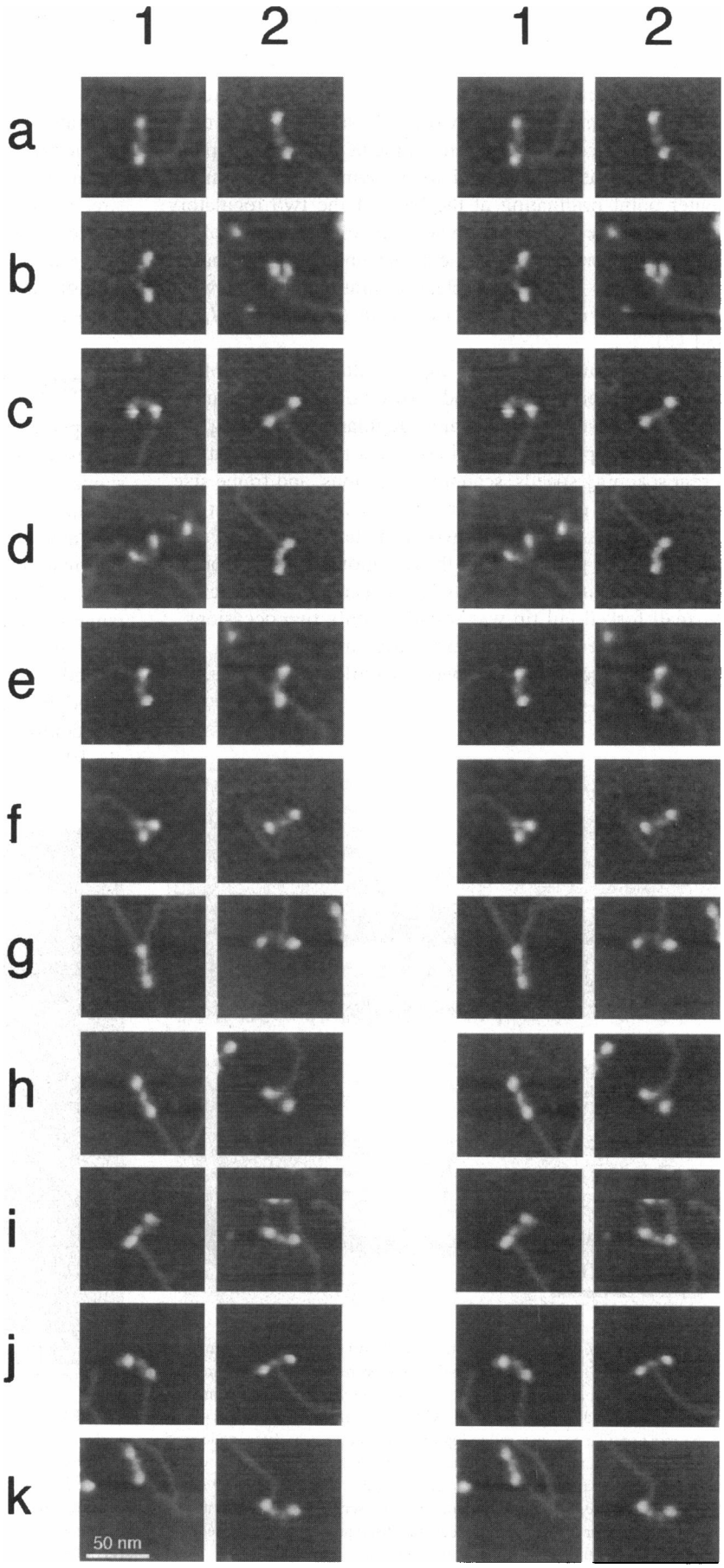

FIGURE 6 Stereoscopic views of 22 myosin molecules showing the regulatory and motor domains of the myosin heads. The contrast is enhanced to maximize detail in the heads, and thus the lower-height tails are not as well visualized in these images. In the majority of these selected molecules, the heads of which are viewed end-on, the heads are separated by 180° and the motor and regulatory domains are well resolved. The motor domain, which has a significantly greater height than the regulatory domain, occupies approximately 50% of a given head. In some images where the heads are viewed from the side, the regulatory domains of adjacent heads are well separated (b1 and d1), and there appears to be unwinding of the coiled-coil at the head-neck juncture. Note in a1, b1, d1, g2, and k2 that a clear separation exists between the regulatory regions of the two heads.

scopic images; for example, in of Fig. 6 *c1*, the heads are bent sharply at the tail juncture and are pointing up toward the viewer. In some images where the heads appear to be viewed from the side, such as *b1* and *d1*, not only were the regulatory domains of the two heads separated, but there appeared to be some unwinding of the tail. Apart from panel *a1*, the two heads appeared to be symmetrical around a center point originating at the base of the two regulatory domains of the two heads. In some images the bases of the two heads were very close, e.g., *h1* and *k1*. Note that in many of these molecules a clear separation exists between the regulatory regions of the two heads (*a1, b1, d1, g1, g2,* and *k2*).

Under optimal conditions, high-resolution images of the myosin tail were obtained and showed distinct modulations of 5–7-nm spacing in the most regular regions (Fig. 7). Although the periodicity varied, it was reproducible at different scanning speeds, scanning directions, and frame size. For example, periodicity can be seen in regions that run parallel to the scan lines in two of the tails shown in Fig. 7 (*arrows*). The periodicity in those regions is 7 nm, consistent with the known 14.1-nm pitch of a coiled-coil structure. A small forked tail tip was found on only two occasions.

In one series of experiments, after myosin in 250 mM ammonium acetate was allowed to settle on the mica, the specimens were vigorously flushed in a stream of H_2O before introducing them into the cryo AFM (Fig. 8). The tails appeared shorter, compared with Fig. 2, and wiggly, with areas where the two strands of the coiled-coil were separated (*arrows*) and the tip of the tail appeared forked (*arrowheads*). The molecules shared a common parallel orientation, presumably reflecting the direction of the stream of H_2O. This unidirectional reorientation of the whole molecules indicates that neither the heads nor the tails are tightly adhered to mica. If heads were selectively strongly attached, one would expect to see tails flipped over the heads or bent in the direction of flow.

DISCUSSION

Comparison of cryo-AFM images of unstained myosin molecules with published electron micrographs of negatively stained or metal-shadowed molecules not only showed sufficient agreement to inspire confidence in this relatively new method, but cryo-AFM of myosin also provided novel information about the effects of thiophosphorylation of MLC_{20}, both long-range (on the tail structure) and short-range (on the flexibility of the head-tail junction of molecules in the 6S conformation). These findings could be related to electron microscopic studies that primarily explored differences between the extended, 6S and the looped, 10S conformers (Onishi and Wakabayashi, 1982; Trybus et al., 1982).

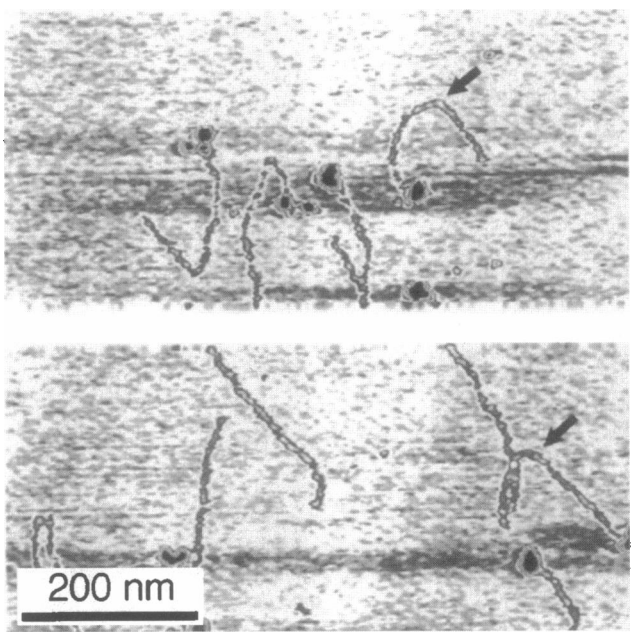

FIGURE 7 Cryo-AFM images of the coiled-coil structure of the smooth-muscle myosin tail. The image has been contrast-reversed, with the tails of the molecules displayed at high gain, resulting in saturation of the images of the myosin heads. The coiled-coil, with a 5–7-nm spacing (14-nm pitch) in the most regular regions, reflecting the heptad repeat of the α-helices of the two myosin heavy chains, can be resolved in the tails. The periodicity was reproducible at different speeds, scanning directions, and frame sizes. Arrows indicate regions that run parallel to the scan lines. The absence of signal in the center of the image reflects the disengagement and subsequent reengagement of the AFM tip with the sample.

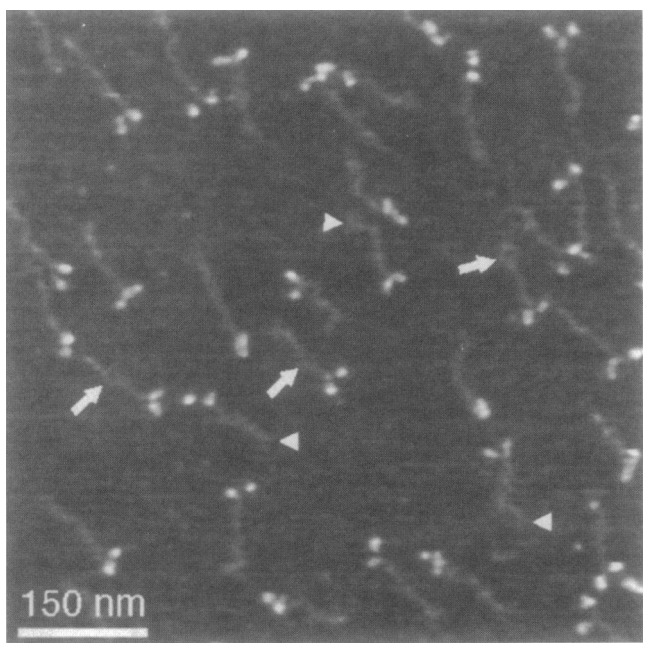

FIGURE 8 Cryo-AFM image of a field of nonphosphorylated myosin molecules. After deposition in 250 mM ammonium acetate on freshly cleaved mica, the specimen was flushed vigorously with a stream of water before introduction into the cryo-AFM. The molecules have reoriented in the direction of the flow, and the interaction in the two α-helices in the tail appear to be weakened and, in some places, well separated (*arrows*). The tips of the tails appear forked in some instances (*arrowheads*).

The predicted length of the tail of gizzard myosin, starting at the beginning of the α-helical/coiled-coil at proline 848 and extending to amino acid 1935, where the paircoil probability (Berger et al., 1995) of a coiled-coil structure drops markedly, is 161 nm (assuming a helical rise of 0.1485 nm/residue for an α-helical coiled-coil; McLachlan and Karn, 1983). The additional 40 amino acids at the COOH terminus of the larger heavy-chain isoform, SM-1, are not helical (rev. in Somlyo, 1993). The tail lengths of nonphosphorylated and thiophosphorylated myosin measured with a Gaussian fit of the distributions were highly significantly different: 154 nm and 150 nm, respectively. Previous studies using electron microscopy of rotary-shadowed molecules have reported tail lengths of 158 nm for chicken gizzard (Onishi and Wakabayashi, 1982), 154 nm ± 9 SD for scallop (Flicker et al., 1983), and 156 nm ± 5 SD for rabbit skeletal myosin (Elliott and Offer, 1978). It could be reasonably expected that, because of shearing of the molecules during the preparative procedures, some tails will be shorter, but not longer, than the predicted length, and that this will give rise to a Gaussian distribution truncated at 161 nm. The data shown in Fig. 2 for the nonphosphorylated myosin tend toward this distribution; the highest value frequency for the nonphosphorylated myosin tail length is at 160 nm, consistent with the lengths predicted from the amino acid sequence. The remaining tail lengths between 160 and 170 nm could reflect the expected small number of longer SM-1 molecules that have extended, albeit nonhelical, tails. The distribution of the thiophosphorylated myosin tail lengths was shifted by 4 nm to shorter values. This was not due to its greater susceptibility to fragmentation, because it was accompanied by a 5-nm shortening between the two major bends in the thiophosphorylated myosin (Fig. 5). Fragmentation would have shortened the distance between the last bend and the tip of the tail, which did not differ significantly in the two populations. The major bend at region II, the S2/LMM site, was 51 and 52 nm from the head-neck junction in the thiophosphorylated and nonphosphorylated myosin, respectively. This is in good agreement with the predicted low probability of coiled-coil structure occurring at 48–51 nm (assuming a 0.1485-nm rise per residue) and is adjacent to a skip residue. The excellent agreement between the 51-nm distance measured from the head-neck junction to region II and the predicted low paircoil score at positions 48–51 nm (based on the amino acid sequence; Berger et al., 1995) suggests that proline 848 is at the head-neck junction, rather than 8 nm within the head portion of the molecule, as had been suggested for *Acanthamoeba* myosin-II (Rimm et al., 1989). This bend was significantly farther than the bend (43 nm) in the tail of the striated muscle myosin molecules measured in rotary-shadowed specimens (Elliott and Offer, 1978). If, as had been suggested (Huxley, 1969; Elliott and Offer, 1978), this bend represents the hinge region that allows the cross-bridge to swing from the shaft of the myosin toward the actin filament, our results would suggest a longer reach and could also contribute to the higher compliance (Warshaw and Fay, 1983) of the cross-bridge in smooth, than in striated, muscles. We note, however, that if both region II (the S2/LMM junction) and the regulatory domain of the head (Rayment et al., 1993a; Uyeda et al., 1996) were to act as hinges, effective transmission of force requires that they not bend on parallel axes.

Decreased coiled-coil probability scores are also predicted at positions 90–93 nm, region III, and 109–110 nm, region IV, from the head-tail junction. The centroid of the distribution of bends in this region was at 95 nm in thiophosphorylated myosin and at 100 nm in nonphosphorylated myosin, suggesting that the nonphosphorylated myosin bends at site IV, which contains a skip residue. Although it seems possible that the thiophosphorylated myosin prefers to bend at site III, which has a low paircoil probability, but no nearby skip residue, we think that this is unlikely, because it would not account for the approximately 4 nm shorter tail length. Alternatively, if bending occurred only at "skip residues" (amino acids 1199 and 1592), thought to alter the pitch of the α-helical coiled-coil (Fig. 5 *A*), the shortening of the distance between the two bends (remaining at the original regions II and IV) could be the result of melting of the coil in that region (see below). Region IV is the position of the hairpin loop in the bent monomeric conformation peculiar to nonphosphorylated vertebrate smooth-muscle myosin in low-ionic-strength solution (Onishi and Wakabayashi, 1982; Trybus et al., 1982; Ikebe and Hartshorne, 1984) and to scallop myosin (Ankrett et al., 1991). Therefore the bend and folding at region IV in nonphosphorylated myosin may be incorrectly positioned for folding in the thiophosphorylated state, where the distance between regions II and IV has decreased by 4 nm. A thiophosphorylation-induced shift of the bend from region IV toward region III (residues 1455–1477, Fig. 5) that corresponds to the hinge III region of Onishi and Wakabayashi (1982) may be a long-range effect that contributes to the lesser propensity of phosphorylated myosin to form the 10S conformer. This conclusion is further supported by the fact that region III is absent (when searched by the paircoil program) in a (scallop) striated muscle myosin that can form a 10S conformer (Ankrett et al., 1991), whereas region IV (labeled as position C by Olney et al., 1996) is present, albeit weakly (minimum paircoil probability 0.728), between residues 1572 and 1590.

Shortening between or within regions II and IV could result from α-helix-random coil transition, as had been proposed to occur, in a different context, at the LMM-S2 junction (region II; Harrington, 1971). The tail length of skeletal myosin decreases by 22 nm over a 17°C increase in temperature (about 1.2 nm/°C), with about half of this shortening occurring between bend positions at 43 nm (II) and 75 nm (IV) from the head-tail junction (Walker et al., 1991). However, we cannot offer an explanation why MLC_{20} phosphorylation would have this effect. Possibly related to the effect of MLC_{20} phosphorylation on tail structure is the report (Levine et al., 1995) showing that phosphorylation of the RLCs of invertebrate and vertebrate

myosin filaments leads to marked disordering of the filament backbone and increased mobility of the myosin heads that moved away from the filament backbone. Phosphorylation of the RLCs may, in addition to switching on the motor, also induce an α-helix to random coil transition in the tail and movement of the heads away from the myosin filament backbone. The interpretation that the shorter tail of thiophosphorylated molecules can be accounted for by the reduced length of the segment between the two major bends is supported by statistical treatment of the data (see above). Nevertheless, it must be treated with some reservations, because the relatively broad distribution of the position of the third bend in nonphosphorylated myosin introduces a greater uncertainty in defining the position of its peak.

A small population (10%) of the tails of both thiophosphorylated and nonphosphorylated myosin had bends in a region close to the head (approximately 24 nm; Figs. 2 *C* and 5) and not predicted by the high paircoil score (1.0). This bend has not been reported previously, but may be related to the observation that smooth-muscle myosin with a less than 27-nm coiled-coil is not a stable structure (Trybus, 1994; Matsu-ura and Ikebe, 1995) and could indicate, together with the greater range of head separations, greater flexibility of cross-bridges when phosphorylated.

We were able to image directly with cryo-AFM the coiled-coil structure, with its 14.1-nm pitch (McLaughlin and Karn, 1982; Quinlan and Stewart, 1987) arising from the hydrophobic interactions of the heavy-chain α-helices. The expected periodicity was best preserved in regions where the tail was roughly parallel to the scan lines, ruling out a scan-line artifact. The variation in periodicity seen in different regions of the tails may also reflect interaction with the negatively charged mica surface, resulting in local changes in the winding of the two α-helices. The width of the tail was about 3.6 nm, broader than the known value of 2.0 nm for two-stranded α-helical coiled-coils, but clearly much closer to the true value than recorded (10–16 nm) with contact imaging of glycerol-spread skeletal-muscle myosin (Hallett et al., 1995). We note that the depth of the groove formed in a coiled-coil by two 1-nm-wide α-helices is only about 0.5 nm. Therefore, visualization of this groove indicates the excellent vertical resolution of the cryo-AFM. Based on this value, at cryogenic temperatures the estimated vertical compression of the myosin tail by the AFM tip is less than 0.5 nm (25%) (Yang et al., 1996). However, the measured height of the tail was only 0.4–0.5 nm, much lower than the actual diameter of a coiled-coil. This reduced height was unlikely to be the result of severe compression, but was probably due to the fact that with the preparatory method used the surface of mica was always covered with 1–2 nm adsorbent that could be scraped away with a stronger cantilever (Han et al., 1995). In other words, the reduced height of the myosin molecules was largely the result of their being partially embedded in the suspension buffer adsorbed to the mica.

The dimensions of nonphosphorylated and thiophosphorylated myosin heads could be measured with cryo-AFM without metal shadowing or negative staining. The lengths of the two populations of myosin heads measured with cryo-AFM, 18.0 $\pm$ 2.5 nm and 18.7 $\pm$ 2.3 nm, as well as the motor domain widths of 9.0 $\pm$ 1.6 nm and 9.5 $\pm$ 1.6 nm, were in good agreement with values obtained with electron microscopy of rotary-shadowed gizzard heavy meromyosin (HMM) (Suzuki et al., 1985), scallop myosin (Flicker et al., 1983), and skeletal-muscle myosin (Elliott and Offer, 1978; Winkelmann and Lowey, 1986), which ranged from 19 to 21 nm in length. In these same studies the width for the gizzard HMM, which was not corrected for the metal shadow, was 11 nm, and the corrected value for the scallop was 8 $\pm$ 1.5 nm, again, similar to the motor domain widths measured with cryo-AFM. These dimensions are slightly larger than the 16.5-nm length, 6.5-nm width, and approximately 4.0-nm thickness reported for the space-filling model of the chicken skeletal-muscle S1 crystal structure, which does not include disordered side chains. The slightly larger width determined by cryo-AFM includes H_2O associated with the molecules and is influenced by the finite size of the AFM tip (Hansma and Hoh, 1994; Shao et al., 1996). The radius of curvature of the tip is believed to be at least several nanometers (Shao et al., 1996). In principle, deconvolution could be applied to remove some of the tip-size effect (Vesenka et al., 1993); however, we did not attempt to apply such procedures, because of the unknown and variable tip size and other problems discussed elsewhere (Shao et al., 1996).

The myosin heads in this and several other studies showed a high degree of variability in the angle between the heads and a given head and the tail. Not only are the heads very flexible, but it has been suggested that each head can rotate independently about the head-tail junction (for a review see Winkelmann and Lowey, 1986; Walker et al., 1991), based on the orientation of antibodies bound to the head and the preponderance of clockwise-curved heads observed in myosin filaments (as well as in isolated molecules). The fewer thiophosphorylated molecules with the heads closely opposed and a greater number with heads separated by 180° are consistent with thiophosphorylation affecting the flexibility of the head-neck junction.

In selected molecules cryo-AFM also revealed separation of the coiled-coil at the base of the heads. This has previously been observed only in rotary-shadowed striated muscle myosin after binding of an antibody to that region (Knight, 1996), again emphasizing the dynamic structure of this junction. Considerable evidence supports the idea that phosphorylation induces a conformational change at the head-neck junction, with the nonphosphorylated "off state" of myosin requiring both regulatory domains (Hasegawa et al., 1990; Trybus, 1994; Cremo et al., 1995) and at least a minimum length of the coiled-coil rod segment (Trybus, 1994; Matsu-ura and Ikebe, 1995). The larger number of nonphosphorylated than thiophosphorylated molecules with close apposition of the two heads would favor interaction of the two RLCs, consistent with these findings.

In high-resolution images of the heads viewed end-on, only two out of 80 molecules (Fig. 6 *a1*) showed the two heads to be offset with the RLCs lying side by side, as had been proposed in a model of striated muscle myosin (Offer and Knight, 1996). The majority of the molecules in this view showed the base of both heads well aligned with no evidence of clockwise curvature, as suggested by the model. Clockwise curvature was observed with molecules viewed from the side. Furthermore, the length of the two heads was twice that of the average 19-nm head length measured in all molecules in a variety of orientations. If side-by-side overlap exists, this length should have been approximately 10 nm shorter. Therefore, our results indicate that the above model is not applicable, at least to the smooth-muscle myosin.

In conclusion, cryo-AFM, even at this early stage of its development, has proved to be a useful and reliable method for imaging single, isolated myosin molecules at a resolution at least comparable to that attainable by electron microscopy. Furthermore, barring an undetectable systematic error that escaped our controls, the application of this method enabled us to detect very small but significant effects of thiophosphorylation of the regulatory light chain on the molecular structure of the extended, 6S conformation of myosin.

We thank Dr. K. Trybus of Brandeis University for kindly providing gizzard smooth muscle myosin; Dr. David Hartshorne, University of Arizona, for providing myosin light-chain kinase and the phosphatase antibody; and Ms. Susan Ramos for gel analysis of the myosin. We acknowledge Dr. W. Han for collecting Fig. 8. We also thank Dr. Jianxun Mou for assistance in instrumentation, Mr. Gang Huang for technical assistance, Mr. Steven Majewski for consultation on statistical analysis, and Ms. Jama Coartney for excellent help with preparation of the figures. We are grateful to Ms. Barbara Nordin for help with preparation of the manuscript.

The work was supported by grants from the National Institutes of Health (RO1-RR07720 and PO1-HL48807).

REFERENCES

Ankrett, R. J., A. J. Rowe, R. A. Cross, J. Kendrick-Jones, and C. R. Bagshaw. 1991. A folded (10S) conformer of myosin from a striated muscle and its implications for regulation of ATPase activity. *J. Mol. Biol.* 217:323–335.

Berger, B., D. B. Wilson, E. Wolf, T. Tonchev, M. Milla, and P. S. Kim. 1995. Predicting coiled coils by use of pairwise residue correlations. *Proc. Natl. Acad. Sci. USA.* 92:8259–8263.

Cremo, C. R., J. R. Sellers, and K. C. Facemyer. 1995. Two heads are required for phosphorylation-dependent regulation of smooth muscle myosin. *J. Biol. Chem.* 270:2171–2175.

Elliott, A., and G. Offer. 1978. Shape and flexibility of the myosin molecule. *J. Mol. Biol.* 123:505–519.

Elmer, T. 1980. Glass surfaces. *In* Silylated Surfaces. D. E. Leiedemin and W. T. Collins, editors. Gordon and Breach, New York. 11–12.

Flicker, P. F., T. Wallimann, and P. Vibert. 1983. Electron microscopy of scallop myosin: location of regulatory light chains. *J. Mol. Biol.* 169: 723–741.

Hallett, P., G. Offer, and M. J. Miles. 1995. Atomic force microscopy of the myosin molecule. *Biophys. J.* 68:1604–1606.

Han, W., J. Mou, J. Sheng, J. Yang, and Z. Shao. 1995. Cryo atomic force microscopy: a new approach for biological imaging at high resolution. *Biochemistry.* 34:8215–8220.

Hansma, H. G., and J. Hoh. 1994. Biomolecular imaging with the atomic force microscope. *Annu. Rev. Biophys. Biomol. Struct.* 23:112–128.

Harrington, W. F. 1971. A mechanochemical mechanism for muscle contraction. *Proc. Natl. Acad. Sci. USA.* 68:685–689.

Hasegawa, Y., K. Tanahashi, and F. Morita. 1990. Regulatory mechanism by the phosphorylation of 20-kDa light chain of porcine aorta smooth muscle myosin. *J. Biochem.* 108:909–913.

Haystead, C. M. M., P. Gailly, A. P. Somlyo, A. V. Somlyo, and T. A. J. Haystead. 1995. Molecular cloning and functional expression of a recombinant 72.5 kDa fragment of the 100 kDa regulatory subunit of smooth muscle protein phosphatase 1 M. *FEBS Lett.* 377:123–127.

Houdusse, A., and P. Cohen. 1995. Structure of the regulatory domain of scallop myosin at 2 Å resolution: implications for regulation. *Structure.* 4:21–32.

Huxley, H. E. 1969. The mechanism of muscular contraction. *Science.* 164:1356–1366.

Ikebe, M., and D. J. Hartshorne. 1984. Conformation-dependent proteolysis of smooth-muscle myosin. *J. Biol. Chem.* 259:11639–11642.

Ikebe, M., and D. J. Hartshorne. 1985. Proteolysis of smooth muscle myosin by *Staphylococcus aureus* protease: preparation of heavy meromyosin and subfragment 1 with intact 20,000-dalton light chains. *Biochemistry.* 24:2380–2387.

Ikebe, M., and D. J. Hartshorne. 1986. Reverse reaction of smooth muscle myosin light chain kinase. *J. Biol. Chem.* 261:8249–8253.

Kitazawa, T., B. D. Gaylinn, G. H. Denney, and A. P. Somlyo. 1991. G-protein-mediated Ca^{2+}-sensitization of smooth muscle contraction through myosin light chain phosphorylation. *J. Biol. Chem.* 266: 1708–1715.

Knight, P. J. 1996. Dynamic behaviour of the head-tail junction. *J. Mol. Biol.* 255:269–274.

Levine, R. J. C., R. W. Kensler, Z. Yang, and H. L. Sweeney. 1995. Myosin regulatory light chain phosphorylation and the production of functionally significant changes in myosin head arrangement on striated muscle thick filaments. *Biophys. J.* 68:224s.

Matsu-ura, M., and M. Ikebe. 1995. Requirement of the two-headed structure for the phosphorylation dependent regulation of smooth muscle myosin. *FEBS Lett.* 363:246–250.

McLachlan, A. D., and J. Karn. 1982. Periodic charge distributions in the myosin rod amino-acid sequence match crossbridge spacings in muscle. *Nature.* 299:226–231.

McLachlan, A. D., and J. Karn. 1983. Periodic features of the amino acid sequence of nematode myosin rod. *J. Mol. Biol* 164:605–626.

Mou, J., J. Yang, and Z. Shao. 1993. An optical detection low temperature atomic force microscope at ambient pressure for biological research. *Rev. Sci. Instrum.* 64:1483–1488.

Offer, G. 1990. Skip residues that correlate with bends in the myosin tail. *Mol. Biol.* 216:213–218.

Offer, G., and P. Knight. 1996. The structure of the head-tail junction of the myosin molecule. *J. Mol. Biol.* 256:407–416.

Olney, J. J., J. R. Sellers, and C. R. Cremo. 1996. Structure and function of the 10 S conformation of smooth muscle myosin. *J. Biol. Chem.* 20375–20384.

Onishi, H., and T. Wakabayashi. 1982. Electron microscopic studies of myosin molecules from chicken gizzard muscle. I. The formation of the intramolecular loop in the myosin tail. *J. Biochem.* 92:871–879.

Onishi, H., T. Wakabayashi, T. Kamata, and S. Watanabe. 1983. Electron microscopic studies of myosin molecules from chicken gizzard muscle. II. The effect of thiophosphorylation of the 20 K-dalton light chain on the ATP-induced change in the conformation of myosin monomers. *J. Biochem.* 94:1147–1154.

Prater, C. B., M. R. Wilson, J. Garnaes, J. Massie, V. B. Elings, and P. K. Hansma. 1991. Atomic force microscopy of biological samples at low temperature. *J. Vac. Sci. Technol.* B9:989–991.

Quinlan, R. A., and M. Stewart. 1987. Crystalline tubes of myosin subfragment-2 showing the coiled-coil and molecular interaction geometry. *J. Cell Biol.* 105:403–415.

Rayment, I., H. M. Holden, M. Whittaker, C. B. Yohn, M. Lorenz, and K. C. Holmes. 1993a. Structure of the actin-myosin complex and its implications for muscle contraction. *Science.* 261:58–65.

Rayment, I., W. R. Rypniewski, K. Schmidt-Bäse, R. Smith, D. R. Tomchick, M. M. Benning, D. A. Winkelmann, G. Wesenberg, and H. M. Holden. 1993b. Three-dimensional structure of myosin subfragment-1: a molecular motor. *Science.* 261:50–58.

Rayment, I., C. Smith, and G. G. Yount. 1995. The active site of myosin. *Annu. Rev. Physiol.* 58:671–702.

Rimm, D. L., J. H. Sinard, and T. D. Pollard. 1989. Location of the head-tail junction of myosin. *J. Cell Biol.* 108:1783–1789.

Shao, Z., J. Mou, D. Czajkowsky, J. Yang, and J. Y. Yuan. 1996. Biological atomic force microscopy: what is achieved and what is needed. *Adv. Physiol.* 45:1–86.

Shao, Z., and A. P. Somlyo. 1995. Stereo representation of atomic force micrographs: optimizing the view. *J. Microsc.* 180:186–188.

Shao, Z., J. Yang, and A. P. Somlyo. 1995. Biological atomic force microscopy: from microns to nanometers and beyond. *Annu. Rev. Cell Dev. Biol.* 11:241–265.

Somlyo, A. P. 1993. Myosin isoforms in smooth muscle: how may they affect function and structure? *J. Muscle Res. Cell Motil.* 14:557–563.

Stafford, W. F., E. M. Szentkiralyi, and A. G. Szent-Györgyi. 1979. Regulatory properties of single-headed fragments of scallop myosin. *Biochemistry.* 24:5273–5280.

Suzuki, H., W. F. Stafford, III, H. S. Slayter, and J. C. Seidel. 1985. A conformational transition in gizzard heavy meromyosin involving the head-tail junction, resulting in changes in sedimentation coefficient, ATPase activity, and orientation of heads. *J. Biol. Chem.* 260: 14810–14817.

Thomson, N. H., M. Fritz, M. Radmacher, J. P. Cleaveland, C. F. Schmidt, and P. K. Hansma. 1996. Protein tracking and detection of protein motion using atomic force microscopy. *Biophys. J.* 70:2421–2431.

Trybus, K. M. 1994. Regulation of expressed truncated smooth muscle myosins. *J. Biol. Chem.* 20819–20822.

Trybus, K. M., T. W. Huiatt, and S. Lowey. 1982. A bent monomeric conformation of myosin from smooth muscle. *Proc. Natl. Acad. Sci. USA.* 79:6151–6155.

Trybus, K. M., and S. Lowey. 1984. Conformational states of smooth muscle myosin. *J. Biol. Chem.* 259:8564–8571.

Tyler, J. M., and D. Branton. 1980. Rotary shadowing of extended molecules dried from glycerol. *J. Ultrastruct. Res.* 71:95–102.

Uyeda, T. Q. P., P. D. Abramson, and J. A. Spudich. 1996. The neck region of the myosin motor domain acts as a lever arm to generate movement. *Proc. Natl. Acad. Sci. USA.* 93:4459–4464.

Vesenka, J., S. Manne, R. Gibberson, T. Marsh, and E. Henderson. 1993. Colloidal gold particles as an incompressible atomic force microscope imaging standard for assessing the compressibility of biomolecules. *Biophys. J.* 65:992–997.

Vibert, P., and C. Cohen. 1988. Domains, motions and regulation in the myosin head. *J. Muscle Res. Cell Motil.* 9:296–305.

Walker, M., P. Knight, and J. Trinick. 1985. Properties of the myosin molecule revealed by negative staining. *J. Mol. Biol.* 184:535–542.

Walker, M., P. Knight, and J. Trinick. 1991. Properties of the myosin molecule revealed by negative staining. *Micron Microsc. Acta.* 22: 413–422.

Warshaw, D. M., and F. S. Fay. 1983. Cross-bridge elasticity in single smooth muscle cells. *J. Gen. Physiol.* 82:157–199.

Whittaker, M., E. M. Wilson-Kubalek, J. E. Smith, L. Faust, R. A. Milligan, and H. L. Sweeney. 1995. A 35-Å movement of smooth muscle mysoin on ADP release. *Nature.* 378:748–751.

Winkelmann, D. A., and S. Lowey. 1986. Probing myosin head structure with monoclonal antibodies. *J. Mol. Biol.* 188:595–612.

Xie, X., and P. Cohen. 1994. Structure of the regulatory domain of scallop myosin at 2.8 Å resolution. *Nature.* 4:27–35.

Yanagisawa, M., Y. Hamada, Y. Katsuragawa, M. Imamura, T. Mikawa, and T. Masaki. 1987. Complete primary structure of vertebrate smooth muscle myosin heavy chain deduced from its complimentary DNA. *J. Mol. Biol.* 198:143–157.

Yang, J., J. Mou, J. Y. Yuan, and Z. Shao. 1996. The effect of deformation on the lateral resolution of atomic force microscopy. *J. Microsc.* 182: 106–113.

Yang, J., and Z. Shao. 1993. The effect of probe force on resolution in atomic force microscopy of DNA. *Ultramicroscopy.* 50:157–170.

Zhang, Y., S. Sheng, and Z. Shao. 1996. Imaging biological structures by the cryo atomic force microscope. *Biophys. J.* 71:2168–2176.